10.1007/s12182-014-0337-2

A seismic texture coherence algorithm and its application

Chuai Xiaoyu[1, 2], Wang Shangxu[1, 2]*, Yuan Sanyi[1, 2], Chen Wei[1, 2] and Meng Xiangcui[1, 2]

[1] State Key Laboratory of Petroleum Resource and Prospecting, China University of Petroleum, Beijing 102249, China
[2] College of Geophysics and Information Engineering, China University of Petroleum, Beijing 102249, China

Abstract: The first generation coherence algorithm (the C1 algorithm) that calculates the coherence of seismic data in-line and cross-line was developed using statistical cross-correlation theory, and it has the limitation that the technique can only be applied to horizons. Based on the texture technique, the texture coherence algorithm uses seismic information in different directions and differences among multiple traces. It can not only calculate seismic coherence in in-line and cross-line directions but also in all other directions. In this study, we suggested first an optimization method and a criterion for constructing the gray level co-occurrence matrix of the seismic texture coherence algorithm. Then the co-occurrence matrix was prepared to evaluate differences among multiple traces. Compared with the C1 algorithm, the seismic texture coherence algorithm suggested in this paper is better than the C1 in its information extraction and application. Furthermore, it implements the multi-direction information fusion and it, also has the advantage of simplicity and effectiveness, and improves the resolution of the seismic profile. Application of the method to field data shows that the texture coherence attribute is superior to that of C1 and that it has merits in identification of faults and channels.

Key words: Texture, coherence, gray level co-occurrence matrix, seismic attribute

1 Introduction

In the interpretation of seismic data, three-dimensional (3-D) seismic attribute is widely applied to the interpretation of geology, faults and structure, identification of porosity, lithology and pore fluids and reservoir characterization (Li et al, 2011a; 2011b; Liu et al, 2011; Meng et al, 2010; Smith, 2010; Tian et al, 2013; Ulvmoen and Omre, 2010; Ulvmoen et al, 2010). From the 1970s to 1980s, three instantaneous seismic attribute based on the Hilbert transform was broadly used in hydrocarbon reservoir exploration. Since the 1990s, the seismic attribute has been utilized for petroleum-gas prediction, reservoir description and four-dimensional seismic monitoring. Therefore, seismic attribute data were used to dynamically monitor reservoir and identify oil and gas (Lewis, 1997). An intelligent algorithm was utilized to choose logging curve parameters which are sensitive to porosity, and these parameters were used as prior information to predict reservoir porosity (Dorrington and Link, 2004). Three-dimensional seismic attribute data were used to predict porosity successfully (Leiphart and Hart, 2001). Core data, logging data and petrophysical data were applied to obtaining the seismic attribute which can be used to identify porosity and faults of reservoir (Fu et al, 2006). Geometric characteristics of the seismic data were utilized to extract coherence properties and curvature attributes which are used to identify complex structures (Sullivan et al, 2006). Three-dimensional seismic attribute technology was used to identify fine geological structure of mineral resources (Manzi et al, 2012). In conclusion, the three-dimensional seismic attribute has been playing an important role in the interpretation of seismic data. At present, there are various kinds of developed seismic attributes. And we know that the most commonly used ones include root-mean-square amplitude, frequency, coherence, AVO and wave impedance (Bing et al, 2012; Liu et al, 2012). Some of these attributes are sensitive to lithology, some are sensitive to fluid, some are sensitive to faults and some are sensitive to channel sand bodies. Through continuous practicing and understanding, researchers generally believe that seismic coherence is one of the most effective and commonly used three-dimensional seismic attributes (Chopra and Marfurt, 2010; Chopra et al, 2011; Marfurt, 2006; Mai et al, 2009). The seismic coherence technique is utilized to interpret seismic data and identify faults and channel sand bodies and it works well.

The seismic coherence technique was first proposed by Bahorich and Farmer in 1995 (Bahorich and Farmer, 1995) and in 1996 they applied for a patent entitled “signal processing and prospecting method”, namely the first

*Corresponding author. email: wangsx@cup.edu.cn
Received April 23, 2013

generation coherence, or C1 for short (Bahorich and Farmer, 1996). In the C1 algorithm, along in-line traces or cross-line traces, every time we take two traces data and then calculate the coherence of these data. Therefore the C1 algorithm is the geometric mean of the coherent attributes of second order statistics of two adjacent in-line traces and two adjacent cross-line traces, but its noise immunity is weak. The second generation coherence technology, or C2 for short, was first proposed in 1998 (Marfurt et al, 1998) and in 1999 the third generation coherence algorithm, or C3 for short, was proposed (Marfurt et al, 1999). In this paper, we only consider improving the C1 algorithm.

Texture is an important characteristic which is used to identify and describe objects in nature. In 1984, texture attribute was introduced into geophysical exploration by Love and Simaan (1984) to process seismic data. However, workers in seismic geology paid little attention to the seismic texture attribute method until West et al (2002) applied texture analysis technology to analyzing 3-D seismic data volume and particularly used artificial neural network technology with texture image analysis technology to process 3-D seismic data volume and quantitatively classify seismic facies. After that, the researchers gradually paid more attention to it. Texture is an important feature utilized to identify objects, and is as important as color and shape. Texture can also be used to identify channel sand bodies and faults. Haralick et al (1973) proposed texture technology in 1973 and used it to recognize and classify images in digital image processing. Texture processing technology based on gray level co-occurrence matrix theory was applied to processing post-stack seismic amplitude data to improve the seismic interpretation resolution in channel sand body recognition and fault interpretation (Gao, 2003; 2009; 2011). In addition, texture processing technology was used to describe and predict reservoir parameters, and for further research into reservoir lithology (Yenugu et al, 2010). In addition a self-organizing map (SOM) algorithm was utilized to analyze 3-D data volume of seismic texture attributes based on a gray level co-occurrence matrix and to study the distribution laws of channel sand bodies (de Matos et al, 2011). Of course, texture technology can be used in other areas as well, such as edge detection (Yang and Luo, 2012; Lu et al, 2012), clustering analysis (Nanthagopal and Rajamony, 2012; 2013), and medical science (Xu et al, 2011), and good application results were obtained.

Post-stack seismic data are digital records which reflect ups and downs of rock stratum, lithological change and physical characteristics of reservoir (Liu and Wang, 2013; Yuan and Wang, 2011). Therefore, post-stack seismic data are the comprehensive responses of imaging laws of the rock stratum. In this paper, we use texture processing technology to describe and study lithology and physical properties which are reflected by seismic amplitude records. It is well known that coherence is an important method to identify faults and channel sand bodies. The coherence analysis technique uses lateral similarity measurement method, and converts ordinary seismic amplitude into another record in similarity metric space by mapping relationship. The first generation coherence algorithm is of great significance and it is simple and practical. However, its anti-noise capacity is poor. The advantage of coherence is to combine kinematics characteristics (travel time) with dynamic characteristics (amplitude) of seismic signals and to clearly show lateral variation of seismic data which is related to geological changes, such as faults, lithofacies changes and channel sand body distribution. In fact, texture is a kind of change or duplicate of image gray value or color space. We can hold the idea that texture is a pattern of grayscale or color changes in a particular form and then they can produce the pattern in the space. Texture is an inherent characteristic of real patterns. Seismic texture attributes contribute to the interpretation of seismogeology, but their capability of identifying small faults, stratigraphic discontinuity, channel sand body distribution and other phenomena is not as good as coherence volume (Chuai et al, 2012; Gao, 2011; Wang et al, 2012). On the basis of texture processing technology, this paper establishes texture coherence to effectively recognize channels and faults. Considering that seismic amplitude is the record of stratified media, the seismic texture coherence algorithm applies gray level co-occurrence matrix to mapping seismic amplitude into image gray value. By using texture technology, the method proposed in this paper establishes an eigenmatrix of dissimilarity so that the seismic texture coherence attribute has the characteristics of multi-trace lateral restraint. This texture technology is used to implement seismic coherence which is based on multi-trace constraints and comprehensively considers the differences and connections of trace data. The characteristic of this method is to apply texture processing technology to converting seismic amplitude data into gray domain. Therefore, various methods which are used to process images can also be utilized to process seismic data. Image processing techniques extend the ways of processing seismic data. The C1 algorithm is simple and effective, and so is the texture coherence algorithm. At the same time, that texture describes layer details of seismic data is introduced into this algorithm. Besides, compared with the first generation coherence algorithm, this method implements multiple directions information fusion which belongs to the data fusion based on characteristic levels. The analysis of cases will show the application of this method.

2 Theories

In the seismic texture coherence algorithm, establishing the gray level co-occurrence matrix is important, and finding the gray level co-occurrence matrix which meets data characteristics is significant as well. In 2002, West et al elaborated the characteristics of the gray level co-occurrence matrix to which seismic event profile corresponds in different sedimentary modes (West et al, 2002), while they did not state the standards and principles of the gray level matrix structure parameters. In this paper, section 2.1 states physical meaning and mathematical definition of gray level co-occurrence matrix. From the perspective of texture feature parameters, section 2.2 and section 2.3 state an optimization method and a criterion which are used to structure the critical parameters of gray level co-occurrence matrix. And on this basis, section 2.4 proposes a seismic texture coherence algorithm and algorithm flow.

2.1 Gray level co-occurrence matrix

Generally speaking, the basic element which constitutes texture is called the texture primitive or texture element. The key point of texture technology is to find the gray level co-occurrence matrix correctly. The gray level co-occurrence matrix is one of the important means applied to analyzing image texture features. According to gray tone level and gray tone direction, we calculate gray correlation between two pixels and then we get the joint probability density function of two locations, namely $p(i, j, d, \theta)$. We use $p(i, j, d, \theta)$ to make up the gray level co-occurrence matrix. This gray level co-occurrence matrix can reflect not only the distribution of texture gray level but also the gray level distribution difference of texture formation structures which have same or similar gray level tone. In fact, the gray level co-occurrence matrix is the second-order statistical characteristic of the image in different gray level tones.

If we define angle as θ, distance as d, the gray level co-occurrence matrix whose gray level is L will be $[p(i, j, d, \theta)]_{L\times L}$. We shall assume that this gray level co-occurrence matrix is adequately specified by the matrix of relative frequency $p(i, j)$ with which two neighboring resolution cells separated by distance d and angle θ occur on the image, one with gray tone i and the other with gray tone j. The gray level matrix of an image shows the general information of the gray related to direction, interval and change, which is defined as following (Haralick et al, 1973),

$$p(i,j,d,\theta)=\#\{((k,l),(m,n))\in(L_y\times L_x)\times(L_y\times L_x)\mid k-m=0,|l-n|=d,I(k,l)=i,I(m,n)=j\} \quad (1)$$

(k, l) and (m, n): pixel coordinates; L_x: row number of images; L_y: column number of images; $\#(x)$: the number of elements in the set x; θ=0°, 45°, 90°, 135°; p: $L\times L$ matrix which is named gray level co-occurrence matrix. The normalized gray level co-occurrence matrix is:

$$R=\begin{bmatrix} p_{0,0} & p_{0,1} & \cdots & p_{0,L-1} \\ p_{1,0} & p_{1,1} & \cdots & p_{1,L-1} \\ \vdots & \vdots & \cdots & \vdots \\ p_{i,0} & p_{i,1} & \cdots & p_{i,L-1} \\ \vdots & \vdots & \ddots & \vdots \\ p_{L-1,0} & p_{L-1,1} & \cdots & p_{L-1,L-1} \end{bmatrix} \quad (2)$$

where L means gray level.

In theory, p can be defined in any direction besides θ=0°, 45°, 90°, 135°, (k, l) and (m, n) can define the gray level co-occurrence matrix, such as $p(i, j, d_a, \theta_a)$, $d_\alpha\in\{D((m,n),(k,l))\}$, where D is the Manhattan distance $\|m-k\|+\|n-l\|$ or linear distance $\sqrt{(m-k)^2+(n-l)^2}$.

2.2 Texture feature parameters of the gray level co-occurrence matrix

In 1973, Haralick defined a variety of texture feature parameters. According to its classification and actual application effect, these are some of the characteristic parameters (Gómez et al, 2012).

1) Sum average. This character reflects the average of the gray scale.

$$f_1=\sum_{i=0}^{n-1}\sum_{i=0}^{n-1} i*p(i,j) \quad (3)$$

2) Sum of squares: Variance. This character reflects gray scale transformation from one point to another.

$$f_2=\sum_i\sum_j (i-\mu)^2*p(i,j) \quad (4)$$

where, μ is the mean of $p(i, j)$.

3) Inverse difference moment. This character reflects local homogeneity.

$$f_3=\sum_i\sum_j \frac{p(i,j)}{1+(i-j)^2} \quad (5)$$

4) Dissimilarity. This character is used to detect the local dissimilarity.

$$f_4=\sum_{i=0}^{n-1}\sum_{j=0}^{n-1}|i-j|\,p(i,j) \quad (6)$$

5) Entropy. This character is a measure of the uncertainty associated with a variable in information theory.

$$f_5=-\sum_i\sum_j p(i,j)*\log(p(i,j)) \quad (7)$$

6) Angular second moment. This character reflects the uniformity of gray level distribution.

$$f_6=\sum_{i=1}^{n}\sum_{j=1}^{n}\left(p(i,j)\right)^2 \quad (8)$$

7) Information measures of correlation.

$$f_{12}=\frac{HXY-HXY1}{\max\{HX,HY\}} \quad (9)$$

where, $HXY=-\sum_i\sum_j p(i,j)*\log(p(i,j))$,

$HXY1=-\sum_i\sum_j p(i,j)*\log\{P_x(i)P_y(j)\}$, HX and HY are entropies of $P_x(i)$ and $P_y(j)$, and the P_x is $P_x=\sum_{j=1}^{n}p(i,j)$, the P_y is $P_y=\sum_{i=1}^{n}p(i,j)$.

Notation:

$p(i, j)$: (i, j)th entry in a normalized gray-tone spatial-dependence matrix.

$p(i)$: ith entry in the marginal-probability matrix obtained by summing the rows of $p(i, j)$,

$$P_x=\sum_{j=1}^{n}p(i,j),$$

$$P_y=\sum_{i=1}^{n}p(i,j).$$

n: number of distinct gray levels in the quantized image.

2.3 Parameter optimization

The gray level co-occurrence matrix is a probability of texture primitives which have positional relationship in statistical space. This probability is related to generation direction, pixel pitch and gray level of gray level co-occurrence matrix. Therefore, it is crucial to determine the gray level co-occurrence matrix formation parameters. In this paper, we have considered all the texture feature parameters from Eq. (3) to Eq. (8), we have discussed the difference between stability and distinction degree of these parameters, and then we have got the direction and distance applied to constructing the gray level co-occurrence matrix, and the selection rules and standards of gray level parameters. The seismic event profile sample is given in Fig. 1, and its texture feature parameters can be found in Haralick's paper. Discussing the stability and discrimination of the texture characteristic parameters, we can get the rules and standards of direction, distance and gray level, which are used to construct the gray level co-occurrence matrix. Of course, texture parameters of different seismic data in different areas need to be selected by using the method provided in this paper.

2.3.1 Samples

Taking into account the texture feature parameters of the following six seismic event profile samples in Fig. 1, we discuss selection criteria and principles of gray level co-occurrence matrix structure parameters in detail.

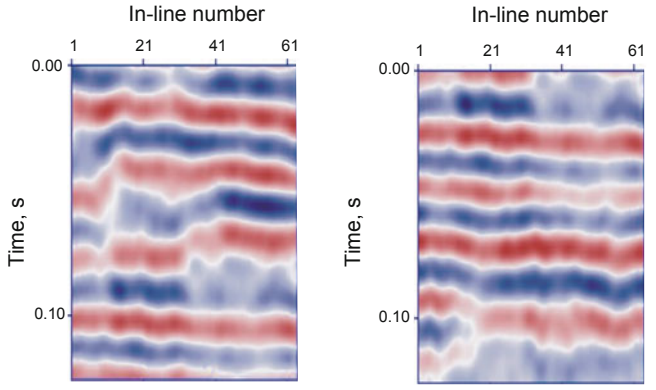

(a) Sample 1 (b) Sample 2

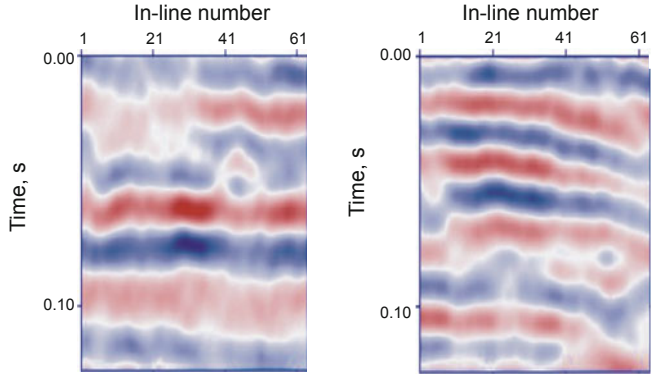

(c) Sample 3 (d) Sample 4

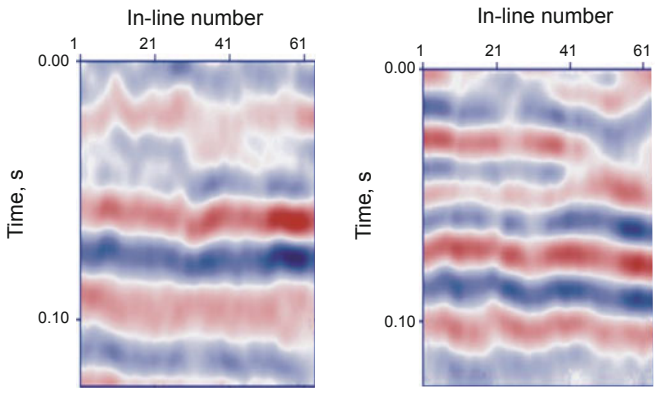

(e) Sample 5 (f) Sample 6

Fig. 1 Seismic event profile samples

2.3.2 Direction parameters

Fig. 2 is the distribution histogram which denotes texture characteristic parameters of samples 1 to 6 in four directions. This figure shows that the characteristic parameters of the same samples in different directions are different. We can qualitatively analyze Fig. 2 and then draw the following conclusions. For one thing, texture feature parameter values dominate in the 0 degree and 90 degree directions. It is consistent with the layered hypothesis of the formation that samples have strong regularity in horizontal and vertical directions. For another, different texture feature parameters have different sensitivity to different samples. In the process of actual calculation, this paper uses weighted value in four directions to select direction parameters in order to ensure the rotation invariance of the parameters.

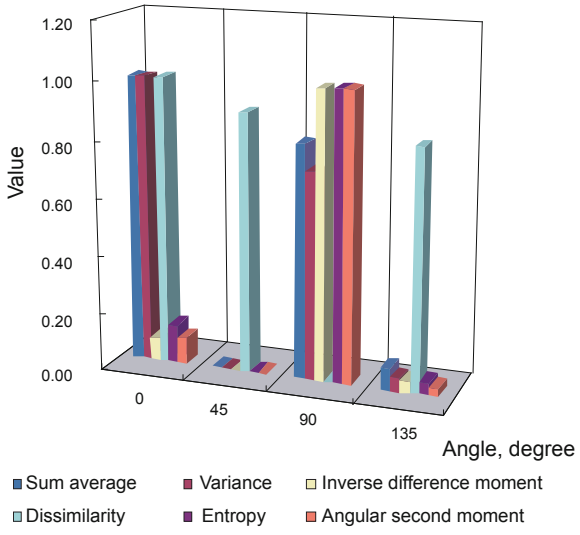

Fig. 2 Distribution histogram of texture feature parameters in different directions

2.3.3 Distance parameters

Fig. 3 illustrates that as the value of the distance parameter increases, the sensitivity of parameter distance discrimination is getting worse from "distance=2" to "distance=14". It can be concluded in Fig. 3 that different characteristic parameters have different sensitivity to different samples. Therefore, the distance parameter which is used to structure gray level co-occurrence matrix can be determined.

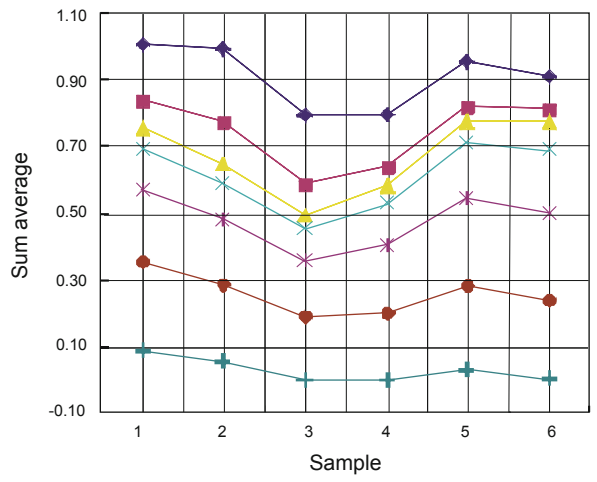

(a) Sum average

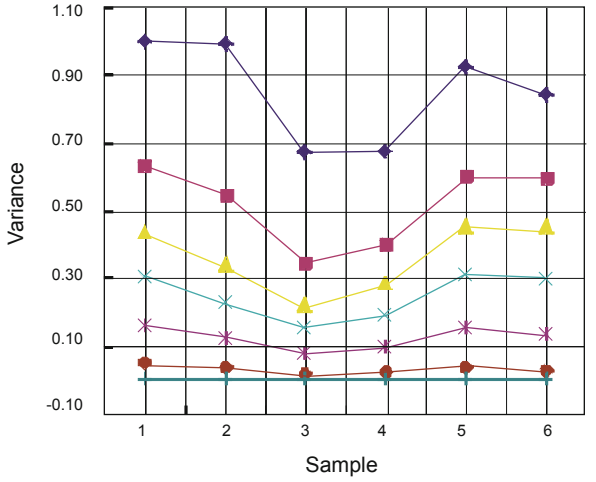

(b) Variance

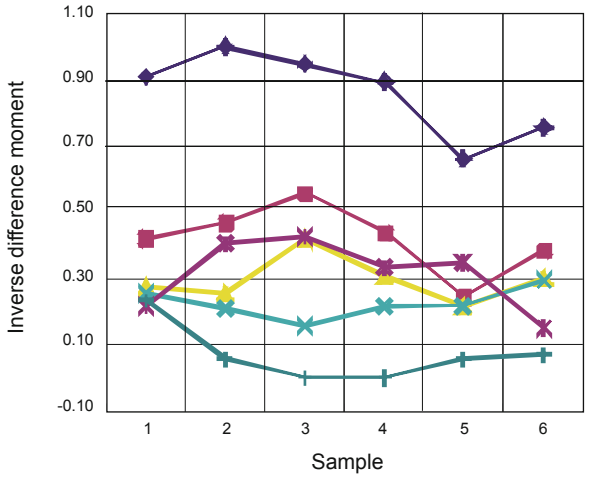

(c) Inverse difference moment

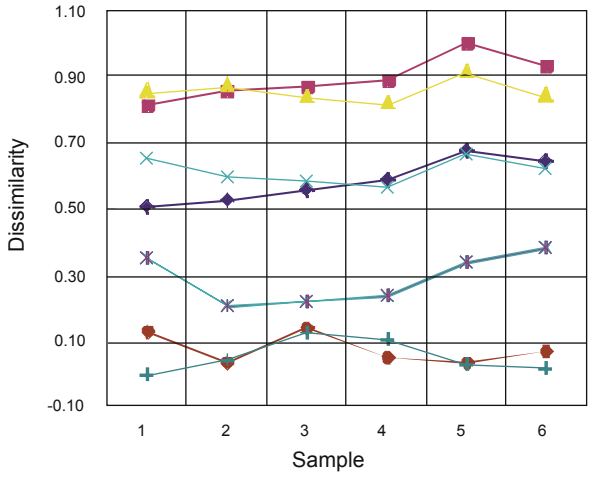

(d) Dissimilarity

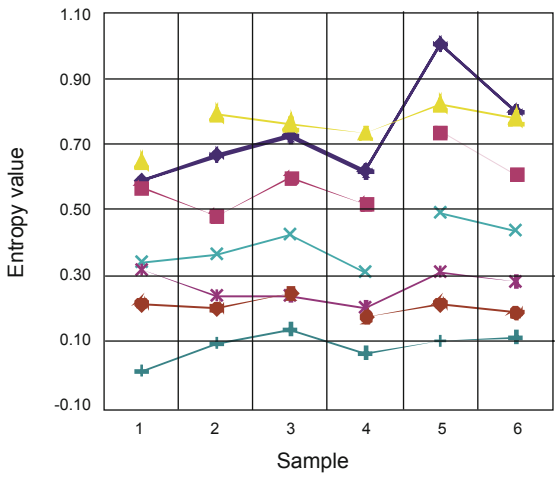

(e) Entropy

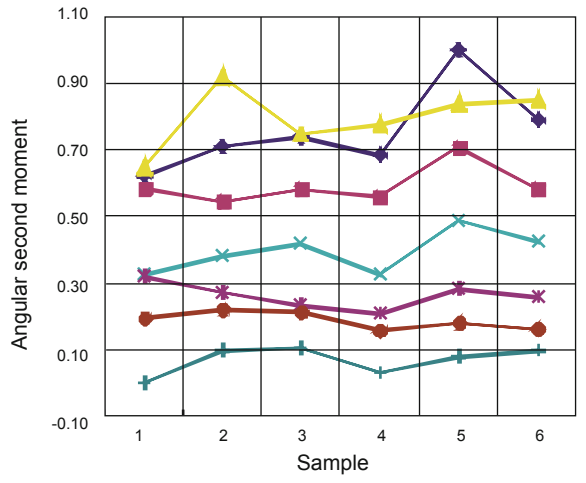

(f) Angular second moment

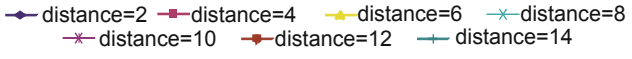

Fig. 3 Scatter diagrams of texture feature parameters and distance change. In Fig. 3, (a) to (f) are scatter diagrams denoting texture feature parameters and distances from sample 1 to sample 6 respectively

2.3.4 Gray level parameters

As is shown in Fig. 4(a), 4(c), 4(e) and 4(f), when the abscissa of the grayscale parameter reaches 16, the resolutions of seismic profiles of different samples become best. When the abscissa is 32, the resolutions follow them. Therefore, one of the important parameters of the gray level co-occurrence matrix is grayscale.

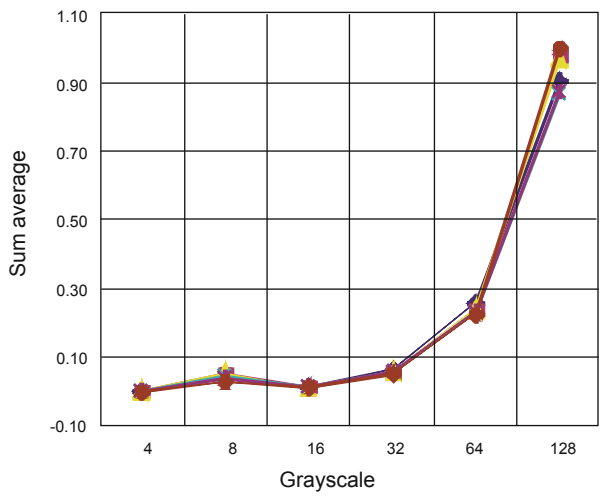

(a) Sum average

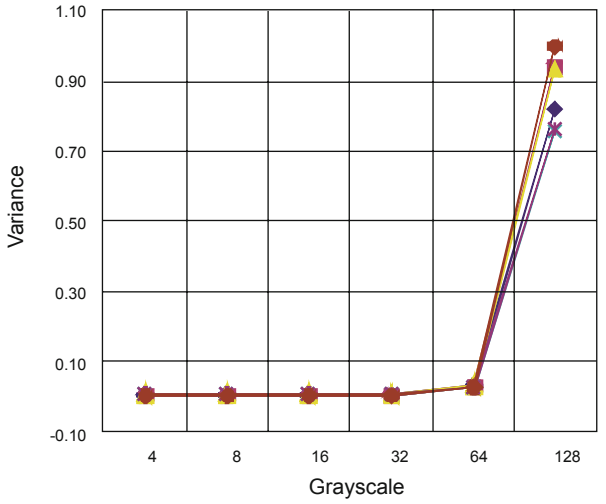

(b) Variance

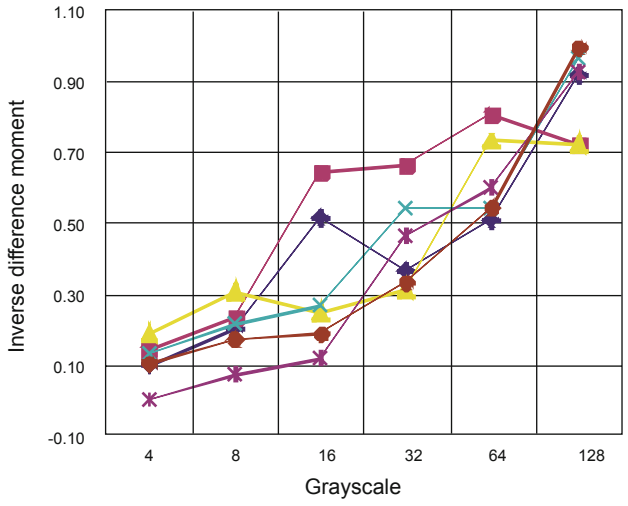

(c) Inverse difference moment

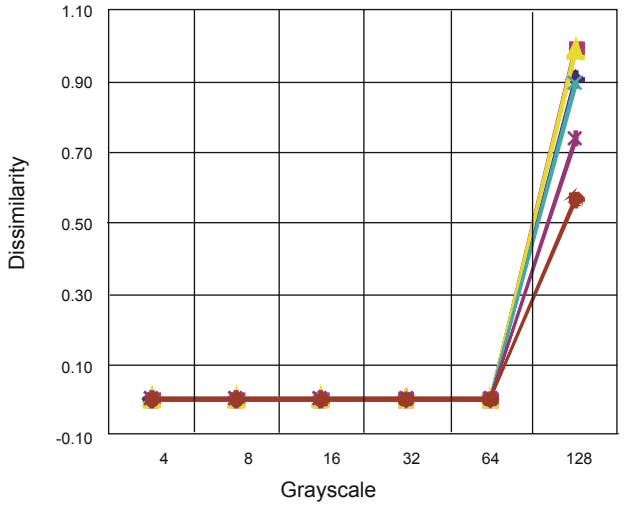

(d) Dissimilarity

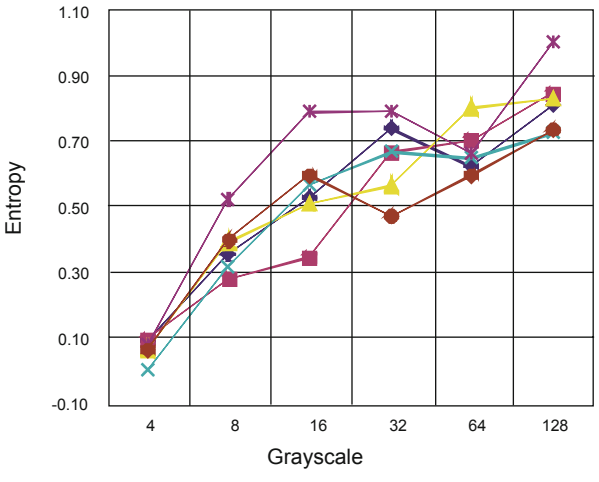

(e) Entropy

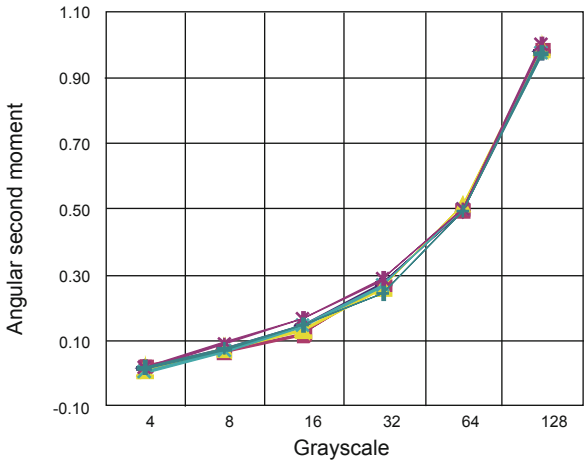

(f) Angular second moment

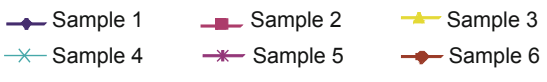

Fig. 4 Scatter diagrams of texture feature parameters and grayscales

2.4 Seismic texture coherence algorithm

In seismic exploration, seismic data or digital records of imaging points record the depth of a subsurface interface and the ups and downs of this interface. Therefore, if we map the seismic data to pixel space through the gray level matrix function, these data can be processed in various methods of digital image processing. In this paper, the gray matrix function of the texture mapping is used to map the seismic data in accordance with different directions and different distances. The relationship among seismic data is considered in new distance space. We define the seismic texture coherence algorithm as follows,

$$\rho(t,\tau,p(d_0,\theta))=\frac{\sum_{k=-K}^{K}\left\{\left[u_0(t+k\Delta t)|_{p(d_0,\theta)}-\mu_0(t)|_{p(d_0,\theta)}\right]\bullet\left[u_1(t+k\Delta t-\tau_x)|_{p(d_0,\theta)}-\mu_1(t-\tau_x)|_{p(d_0,\theta)}\right]\right\}}{\left\{\sum_{k=-K}^{K}\left[u_0(t+k\Delta t)|_{p(d_0,\theta)}-\mu_0(t)|_{p(d_0,\theta)}\right]^2\bullet\sum_{k=-K}^{K}\left[u_1(t+k\Delta t-\tau_x)|_{p(d_0,\theta)}-\mu_1(t-\tau_x)|_{p(d_0,\theta)}\right]^2\right\}} \tag{10}$$

where, $\mu_m=\frac{1}{2K+1}\sum_{k=-K}^{K}u_m(t+k\Delta t)$, denotes the average value of mth trace in the time window analyzed, Δt is the time lag, and $2k$+1 is the number of samples in the window, $p(d_0, \theta)$ denotes the gray level matrix in which d_0 is the distance and θ is the direction, u_m is the mth trace of original seismic data within the time window analyzed. Finally, we have the texture coherence attribute of a 3-D seismic data cube,

$$c|_{(\tau,p(d_0,\theta))}=\sqrt{\left(\max\rho|_{(\tau,p(d_0,0^\circ))}\right)\bullet\left(\max\rho|_{(\tau,p(d_0,45^\circ))}\right)\bullet\left(\max\rho|_{(\tau,p(d_0,90^\circ))}\right)\bullet\left(\max\rho|_{(\tau,p(d_0,135^\circ))}\right)} \tag{11}$$

where, $\max\rho|_{(\tau,p(d_0,\theta))}=\max(\rho(t,\tau,p(d_0,\theta)))|_{(\tau,p(d_0,\theta))}$.

The whole algorithm flow is summarized as follows:

1) Pre-process post-stack seismic amplitude data: remove noise with seismic event edges preserved, and enhance resolution (Yuan and Wang, 2013a; 2013b).

2) Establish the gray level co-occurrence matrix and initialize θ, d and L.

3) Calculate texture characteristic parameters.

4) According to the texture characteristic parameters, refine matrix parameters of the gray level co-occurrence matrix: θ, d and L.

5) Calculate the matrix parameters of the gray level co-occurrence matrix. If they are reasonable, go to step 6, otherwise go to step 2.

6) Use Eqs. (10)-(11) to calculate the texture coherence.

7) Output the results.

The 3-D seismic texture coherence data volumes which are obtained from the workflows above are used to identify channels and faults. In order to test the effectiveness of this algorithm, it is applied to field data of an oilfield in China to identify the channel sand bodies and faults. And we will give a practical example in the next section.

3 Cases

In our study, practical 3-D seismic data from an oil field is used to test the algorithm. The target area is mainly shore-shallow lake with sedimentation occurring in arid and semiarid climates. Then the lake basin spreaded, the lake bottom was uplifted and some meanders developed. The channel sand in this area is thin and the channels are narrow, which makes the channel features hard to see and makes it difficult to identify channels from seismic sections alone (Fig. 5). It is a typical micro-amplitude structure and lithology trap complex reservoir.

As we can see in Fig. 5, profile Pa is along channel seismic lineup profiles, while profiles Pb, Pc and Pd are perpendicular to the channel. In profiles Pb, Pc and Pd, we can hardly see seismic event characteristics which would be convex or concave in the direction of vertical channel sands, which is caused by the thin and narrow channel sand bodies. Therefore, it is difficult for conventional seismic attributes to identify the target geological body. In Fig. 5, the data framed by red area are applied to acting as test data of this paper. The analysis of the results will be given from Fig. 6 to Fig. 9 below.

In this paper, we choose the amplitude attributes that are sensitive to channels and faults in the area. Fig. 6 is the maximum amplitude attribute, and the outline of the channels is vague. The channel boundaries are hard to distinguish and there is almost no response of the northeast-southwest fault F3. Fault F1 and fault F2 are not separated from each other in Fig. 6. Also fault F4 associated with fault F3 cannot be identified.

Fig. 7 shows the texture information attribute which is extracted by using the texture algorithm. In this figure, the outline of the channel is evident (the black dashed lines are the boundaries of the channel), and the nearly northwest-southeast fault F1 and fault F2 and the northeast-southwest fault F3 are all clearer than those in Fig. 6. However, it is still hard to identify fault F4.

Amplitude or texture attributes cannot clearly identify channel sand bodies and faults of complex structure areas.

Fig. 8 shows the coherence which is extracted by the first generation coherence algorithm, in which the channel has mid-strong or strong values surrounded with relatively low values. The boundary of the channel is clear and we can clearly see the extension features of the channel (dashed lines are its boundaries). The nearly northeast-southwest fault F3 and nearly northwest-southeast fault F2 are clear in the figure. However, fault F1 and fault F4 are not clear in this attribute slice.

Fig. 9 shows the seismic texture coherence slice obtained by using the method given in this paper. In Fig. 9, the channel has strong values with surrounding low values. The difference between the sand in the channel and the mud stone is much more apparent in the seismic texture coherence slice than in seismic coherence slice, resulting in the clearer outline of the channel (dashed lines are its boundaries). In comparison with the maximum amplitude in Fig. 6 and the texture attribute in Fig. 7, the seismic texture coherence shown in Fig. 9 is more effective in identifying the boundaries of the channel. The faults which cannot be identified in Fig. 6 and Fig. 7 are distinguishable in Fig. 9. Compared with the seismic coherence in Fig. 8, fault F4 in Fig. 9 is still not depicted very clearly. But the response characteristics of fault F1, F2 and F3 are much superior to those in Fig. 8. Especially, the faults F1 and F2 crosscut the channel in Fig. 9, while this crosscutting feature is not obvious in Fig. 8.

There is evidence in the corresponding seismic profiles shown in Fig. 10 and Fig. 11. In the event profile P1 in Fig. 10, the events break at F3, which prove that the interpretation of fault F3 in Fig. 8 and Fig. 9 is reasonable. The similar evidence that the events cross and joint at the locations of fault F1 and F2 can also be found in profile P3 shown in Fig. 11(b). In profile P2 in Fig. 11(a), the events break and the train of waves is discontinuous at fault F3 and F4, and

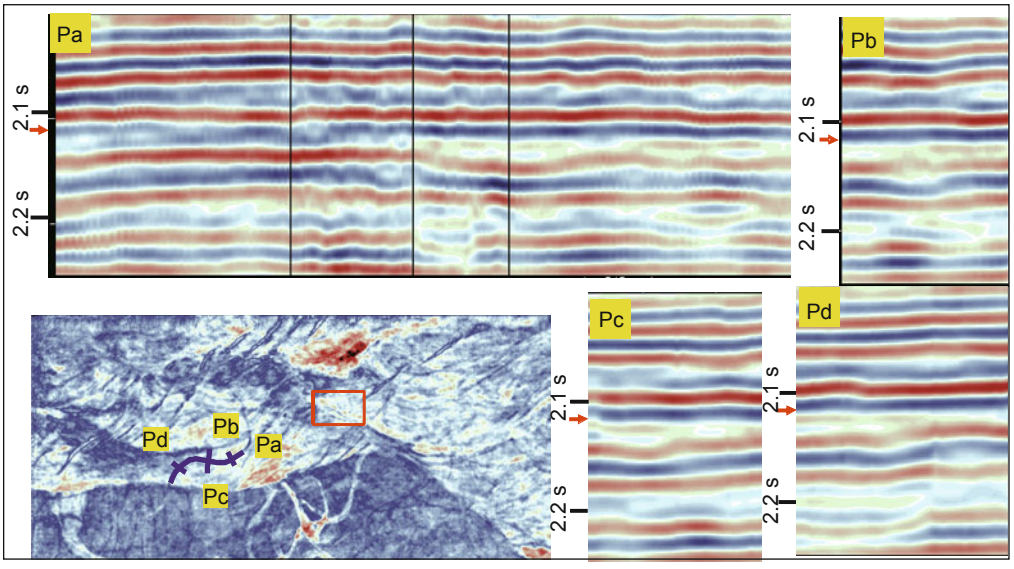

Fig. 5 Channels and seismic event profiles. In Fig. 5, profile Pa is the seismic event profile along channels; profiles Pb, Pc and Pd respectively are seismic event profiles which are perpendicular to the channel from top to bottom; the red arrow points to the target horizon; the area delineated by the red rectangle is the data area which is tested by the seismic texture coherence algorithm proposed in this paper

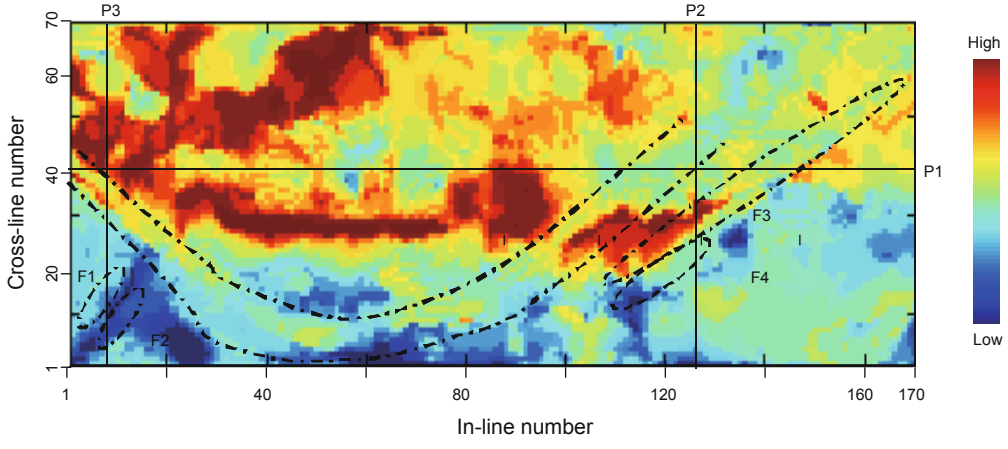

Fig. 6 The maximum amplitude attribute slice. In Fig. 6, P1 is the location of seismic event profile P1 in Fig. 10; P2 is the location of seismic event profile P2 in Fig. 11(a); P3 is the location of seismic event profile P3 in Fig. 11(b); the brown ellipses F1, F2, F3, F4 are the serial numbers of the faults; black dashed lines are the boundaries of the channel

thus it is reasonable to draw a fault here. Therefore, the fault location and its direction, which are interpreted according to the attribute (Fig. 9) calculated by the algorithm studied in this paper, are reliable. This example shows that both channel and faults of field data can be successfully identified by using the seismic texture coherence algorithm.

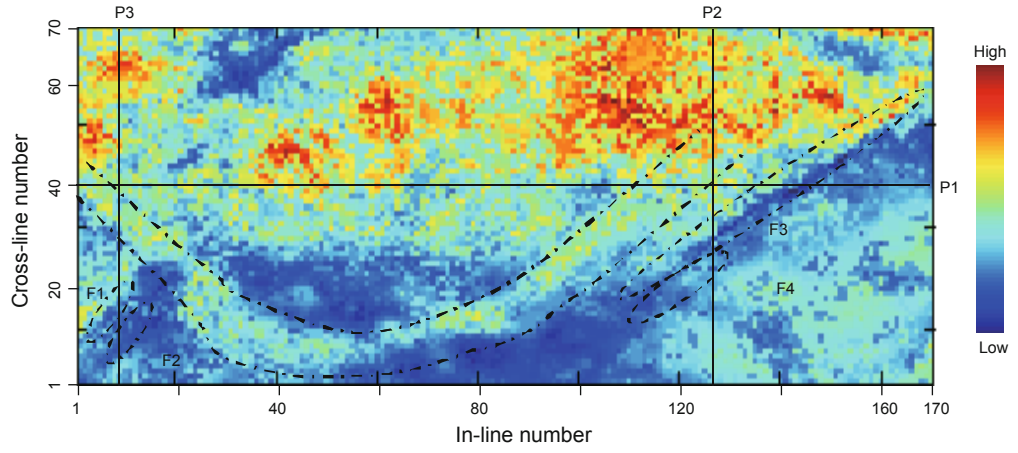

Fig. 7 Texture information attribute slice. In Fig. 7, P1 shows the location of seismic event profile P1 in Fig. 10; P2 is the location of seismic event profile P2 in Fig. 11(a); P3 is the location of seismic event profile P3 in Fig. 11(b); the brown ellipses F1, F2, F3, F4 are the serial numbers of the faults; black dashed lines are the boundaries of the channel

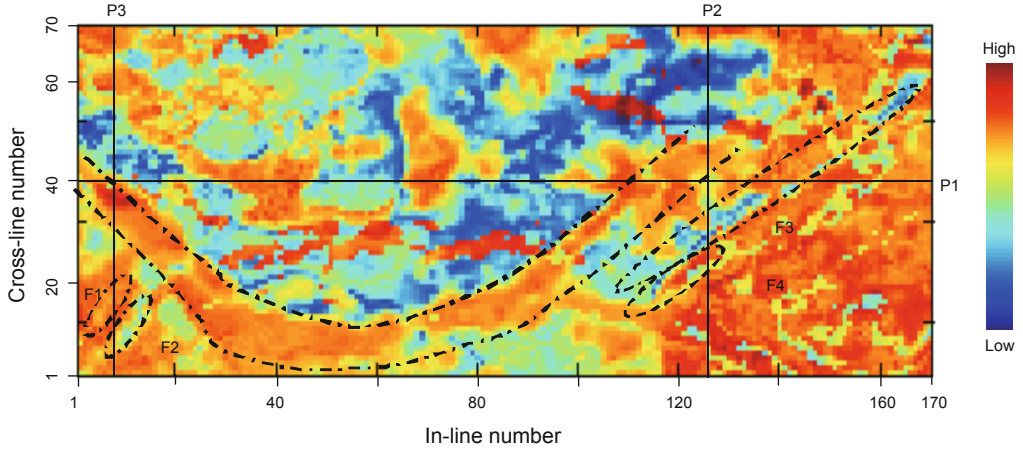

Fig. 8 The first generation coherence attribute slice. In Fig. 8, P1 shows the location of seismic event profile P1 in Fig. 10; P2 is the location of seismic event profile P2 in Fig. 11(a); P3 is the location of seismic event profile P3 in Fig. 11(b); the brown ellipses F1, F2, F3, F4 are the serial numbers of the faults; black dashed lines are the boundaries of the channel

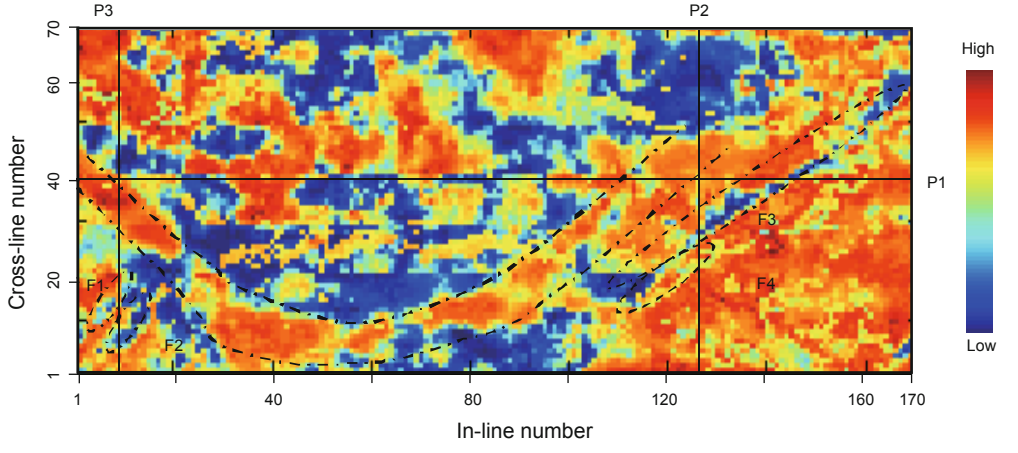

Fig. 9 Seismic texture coherence attribute slice. In Fig. 9, P1 is the location of seismic event profile P1 in Fig. 10; P2 shows the location of seismic event profile P2 in Fig. 11(a); P3 is the location of seismic event profile P3 in Fig. 11(b); the brown ellipses F1, F2, F3, F4 are the serial numbers of the faults; black dashed lines are the boundaries of the channel

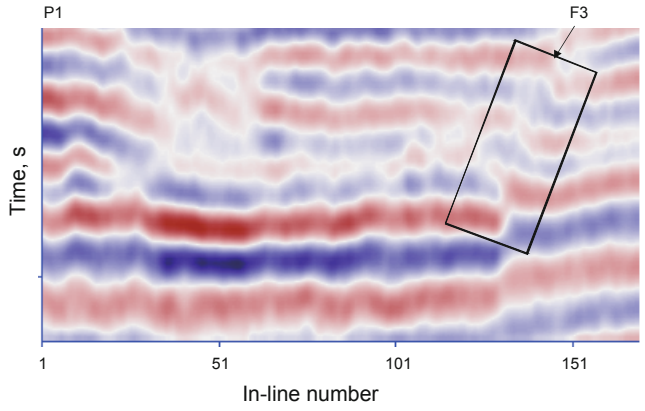

Fig. 10 Seismic event profile P1

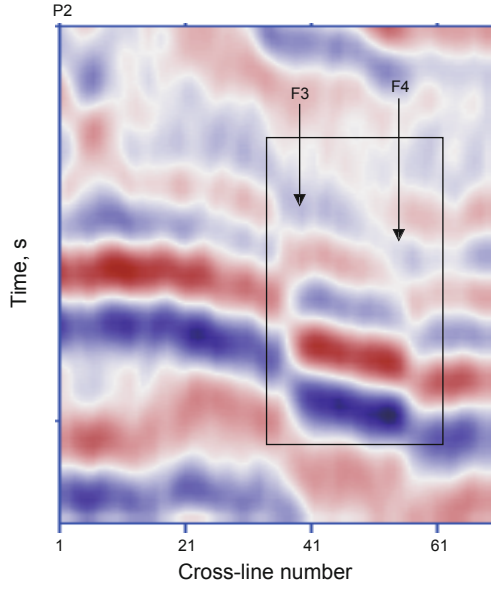

(a) Profile P2

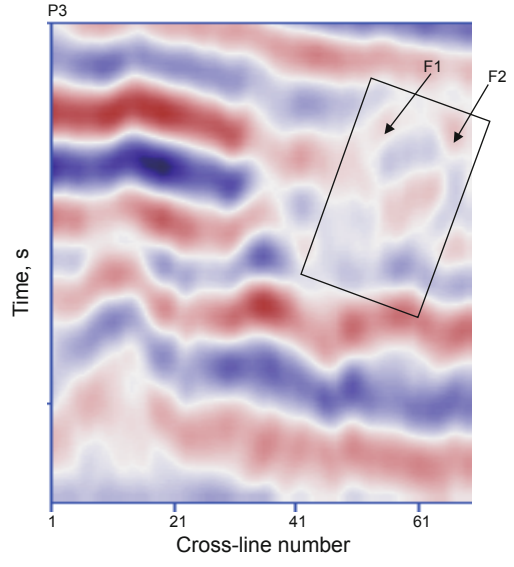

(b) Profile P3

Fig. 11 Seismic event profiles P2 and P3

4 Conclusions

In this study, seismic attribute analysis techniques are applied to fault and channel identification in clastic reservoir exploration and development. On the basis of previous research results, the texture coherence algorithm of seismic attribute has been suggested and generalized to fault and channel identification and quantative evaluation. It implements information fusion of many directions and lateral constraint of multiple traces, and it first clearly proposes an optimization method and a criterion used to build gray level co-occurrence matrix parameters in the seismic texture coherence algorithm. The process utilized to select texture parameters of gray level co-occurrence matrix is universal. This algorithm has advantages over the first generation coherence algorithm in following two aspects.

1) To combine the three types of parameters (different directions, gray tone level and distance), we use the mapping function of the gray level co-occurrence matrix usually deployed in texture processing technology to transfer the seismic amplitude records into texture attributes. This is the foundation of the seismic texture coherence algorithm suggested in this paper.

2) The texture coherence algorithm has some of the merits of the C1 algorithm in conciseness and computational efficiency. Moreover, it also has advantages in information fusion in many directions and multiple traces, and it enhances the resolution of faults and channel identification.

Field applications show that the method suggested in this paper has better resolution and can show in detail complex geological targets. Therefore, the method lays a sound foundation for identifying and evaluating complex geologic bodies using seismic data.

Acknowledgements

We are grateful to the anonymous referees for their comments on this paper. We also thank our professors and classmates from the CNPC Key Laboratory for their help. This research is supported by National “973” Program (No. 2013CB228600).

References

Bahorich M and Farmer S. 3-D seismic discontinuity for faults and stratigraphic features: The coherence cube. The Leading Edge. 1995. 14(10): 1053-1058

Bahorich M and Farmer S. Apparatus for seismic signal processing and exploration. 1996. US Patent 5838564

Bing P P, Cao S Y and Lu J T. Non-linear AVO inversion based on support vector machine. Chinese Journal of Geophysics. 2012. 55(3): 1025-1032 (in Chinese)

Chopra S and Marfurt K J. Integration of coherence and volumetric curvature images. 80th Annual International Meeting, SEG Technical Program Expanded Abstracts. 2010. 1281-1286

Chopra S, Misra S and Marfurt K J. Coherence and curvature attributes on preconditioned seismic data. The Leading Edge. 2011. 30(4): 386-393

Chuai X Y, Wang S X, Shen J S, et al. A new seismic coherence cube algorithm: Seismic texture coherence algorithm. 82th Annual International Meeting, SEG Technical Program Expanded Abstracts.

2012. 1-5

de Matos M C, Yenugu M, Angelo S M, et al. Integrated seismic texture segmentation and cluster analysis applied to channel delineation and chert reservoir characterization. Geophysics. 2011. 76(5): P11-P21

Dorrington K P and Link C A. Genetic-algorithm/neural-network approach to seismic attribute selection for well-log prediction. Geophysics. 2004. 69(1): 211-221

Fu D, Sullivan E C and Marfurt K J. Rock-property and seismic-attribute analysis of a chert reservoir in the Devonian Thirty-one Formation, west Texas, U.S.A.. Geophysics. 2006. 71(5): B151-B158

Gao D L. Volume texture extraction for 3D seismic visualization and interpretation. Geophysics. 2003. 68(4): 1294-1302

Gao D L. 3D seismic volume visualization and interpretation: An integrated workflow with case studies. Geophysics. 2009. 74(1): W1-W12

Gao D L. Latest developments in seismic texture analysis for subsurface structure, facies, and reservoir characterization: A review. Geophysics. 2011. 76(2): W1-W13

Gómez W, Pereira W C A and Infantosi A F C. Analysis of co-occurrence texture statistics as a function of gray-level quantization for classifying breast ultrasound. IEEE Transaction on Medical Imaging. 2012. 31(10): 1889-1899

Haralick R M, Shanmugam K and Dinstein I H. Textural features for image classification. IEEE Transaction on Systems, Man and Cybernetics. 1973. 3(6): 610-621

Lei phart D J and Hart B S. Comparison of linear regression and a probabilistic neural network to predict porosity from 3-D seismic attributes in Lower Brushy Canyon channeled sandstones, southeast New Mexico. Geophysics. 2001. 66(5): 1349-1358

Lewis C. Seismic attributes for reservoir monitoring: A feasibility study using forward modeling. The Leading Edge. 1997. 16(5): 459-470

Li G F, Li H, Ma Y Y, et al. Analysis of the ambiguity of log-constrained seismic impedance inversion. Petroleum Science. 2011a. 8(2): 151-156

Li W G, Bhattacharya J P and Wang Y M. Delta asymmetry: Concepts, characteristics, and depositional models. Petroleum Science. 2011b. 8(3): 278-289

Liu L F, Sun S Z, Yang H J, et al. Seismic attributes and integrated prediction of fractured and caved carbonate reservoirs in the Tarim Basin, China. Petroleum Science. 2011. 8(2): 455-461

Liu Y, Zhang J S, Hu G M, et al. A study of the three-term non-Gaussian pre-stack inversion method. Chinese Journal of Geophysics. 2012. 55(1): 55-64 (in Chinese)

Liu Z W and Wang Y C. A joint high-resolution processing method and its application for thin inter-beds. Petroleum Science. 2013. 10(1): 195-204

Love P L and Simaan M. Segmentation of stacked seismic data by the classification of image texture. 54th Annual International Meeting, SEG Technical Program Expanded Abstracts. 1984. 480-482

Lu Y H, Lu W K and Zhai Z J. An edge-preserving seismic data interpolation method. Chinese Journal of Geophysics. 2012. 55(3): 991-997 (in Chinese)

Mai H T, Marfurt K J and Chávez-Pérez S. Coherence and volumetric curvatures and their spatial relationship to faults and folds, an example from the Chicontepec Basin, Mexico. 79th Annual International Meeting, SEG Technical Program Expanded Abstracts. 2009. 1063-1067

Manzi M S D, Gibson M A S, Hein K A A, et al. Application of 3D seismic techniques to evaluate ore resources in the West Wits Line goldfield and portions of the West Rand goldfield, South Africa. Geophysics. 2012. 77(5): WC163-WC171

Marfurt K J. Robust estimates of 3D reflector dip and azimuth. Geophysics. 2006. 71(4): P29-P40

Marfurt K J, Kirlin R L, Farmer S L, et al. 3-D seismic attributes using a semblance-based coherency algorithm. Geophysics. 1998. 63(4): 1150-1165

Marfurt K J, Sudhaker V, Gersztenkorn A, et al. Coherency calculations in the presence of structural dip. Geophysics. 1999. 64(1): 104-111

Meng Y L, Liang H W, Meng F J, et al. Distribution and genesis of the anomalously high porosity zones in the middle-shallow horizons of the northern Songliao Basin. Petroleum Science. 2010. 7(3): 302-310

Nanthagopal A P and Rajamony R S. Automatic classification of brain computed tomography images using wavelet-based statistical texture features. Journal of Visualization. 2012. 15(4): 363-372

Nanthagopal A P and Rajamony R S. Classification of benign and malignant brain tumor CT images using wavelet texture parameters and neural network classifier. Journal of Visualization. 2013. 16(1): 19-28

Smith M. Rock property inversion for carbonate porosity in the Edwards reef complex. 80th Annual International Meeting, SEG Technical Program Expanded Abstracts. 2010. 368-372

Sullivan E C, Marfurt K J, Lacazette A, et al. Application of new seismic attributes to collapse chimneys in the Fort Worth Basin. Geophysics. 2006. 71(4): B111-B119

Tian Y K, Zhou H and Yuan S Y. Lithologic discrimination method based on Markov random-field. Chinese Journal of Geophysics. 2013. 56(4): 1360-1368 (in Chinese)

Ulvmoen M and Omre H. Improved resolution in Bayesian lithology/fluid inversion from prestack seismic data and well observations: Part 1—Methodology. Geophysics. 2010. 75(2): R21-R35

Ulvmoen M, Omre H and Buland A. Improved resolution in Bayesian lithology/fluid inversion from prestack seismic data and well observations: Part 2—Real case study. Geophysics. 2010. 75(2): B73-B82

Wang Z G, Yin C, Lei X L, et al. GLCM parameters in fluvial texture analysis. Oil Geophysical Prospecting. 2012. 47(1): 100-106 (in Chinese)

West B P, May S R, Eastwood J E, et al. Interactive seismic facies classification using textural attributes and neural networks. The Leading Edge. 2002. 21(10): 1042-1049

Xu S F, Wu S L and Li H. An analysis on human skin texture based on gray-level co-occurrence matrix. Acta Laser Biology Sinica. 2011. 20(3): 324-328 (in Chinese)

Yang H and Luo Y. Gray level co-occurrence matrix-based edge detection algorithm. Intelligent Computer and Applications. 2012. 2(6): 43-45 (in Chinese)

Yenugu M, Marfurt K J and Matson S. Seismic texture analysis for reservoir prediction and characterization. The Leading Edge. 2010. 29(9): 1116-1121

Yuan S Y and Wang S X. A local *f-x* Cadzow method for noise reduction of seismic data obtained in complex formations. Petroleum Science. 2011. 8(3): 269-277

Yuan S Y and Wang S X. Spectral sparse Bayesian learning reflectivity inversion. Geophysical Prospecting. 2013a. 61(4): 735-746

Yuan S Y and Wang S X. Edge-preserving noise reduction based on Bayesian inversion with directional difference constraints. Journal of Geophysics and Engineering. 2013b. 10(2): 1-10

(Edited by Hao Jie)